RSC Advances

PAPER

View Article Online
View Journal | View Issue

Cite this: *RSC Adv.*, 2020, **10**, 1219

Rapid and selective electrochemical transformation of ammonia to N_2 by substoichiometric TiO_2-based electrochemical system†

Yanbiao Liu, *[ab] Jiancheng Mei,[a] Chensi Shen,[ab] Manhong Huang,[ab] Ming Yang,[c] Zhiwei Wang,[bd] Wolfgang Sand[ae] and Fang Li*[ab]

Received 16th September 2019
Accepted 19th December 2019

DOI: 10.1039/c9ra07470h

rsc.li/rsc-advances

In this study, we have developed a continuous-flow electrochemical system towards the rapid and selective conversion of ammonia to N_2, based on a tubular substoichiometric titanium dioxide (Ti_4O_7) anode and a Pd–Cu co-modified Ni foam (Pd–Cu/NF) cathode, both of which are indispensable. Under the action of a suitable anode potential, the Ti_4O_7 anode enables the conversion of Cl^- to chloride radicals ($Cl^\bullet$), which could selectively react with ammonia to produce N_2. The anodic byproducts, *e.g.* NO_3^-, were further reduced to N_2 at the Pd–Cu/NF cathode. EPR and scavenger experiments confirmed the dominant role of $Cl^\bullet$ in ammonia conversion. Complete transformation of 30 mg L^{-1} ammonia could be obtained over 40 min of continuous operation under optimal conditions. The proposed electrochemical system also exhibits enhanced oxidation kinetics compared to conventional batch systems. This study provides new insights into the rational design of a high-performance electrochemical system to address the challenging issue of ammonia pollution.

1. Introduction

The excessive discharge of ammonia wastewater accelerates the eutrophication of water bodies and causes the serious water pollution we are currently facing.[1–3] To address this issue, various radical-based catalytic processes have been extensively studied.[4–6] The hydroxyl radical ($OH^\bullet$) and sulfate radical ($SO_4^{-\bullet}$) are two types of highly potent radicals that have been widely applied. However, another important but often neglected type of radical, chloride radicals ($Cl^\bullet$), have received only limited attention. These $Cl^\bullet$ are selective oxidants ($E^0 = 2.4$ V *vs.* NHE) that react with electron-rich groups like ammonia through single electron oxidation, H-abstraction, and addition to unsaturated C–C bonds.[7,8] We have previously developed a flow-through electrochemical system enabling the sustainable production of $Cl^\bullet$ and further converting ammonia to N_2.[9] Unfortunately, the poor stability of the SnO_2-modified carbon nanotube anode under elevated anode potentials significantly limits its wide application. In separate study, Zhang *et al.* employed a coupled Ti/IrO_2–RuO_2 anode and a Ti cathode and also achieved conversion of ammonia into N_2 within a conventional batch reactor.[10] They believed that the produced active chlorine was responsible for the oxidation of ammonia. But the treatment kinetics were far from satisfactory. It is, therefore, highly desirable to develop efficient, environmentally friendly and affordable electrochemical systems for ammonia decontamination.

In recent years, Magnéli phase titanium sub-oxides have been considered as promising electrode materials for electrochemical applications, due to their increased electrical conductivity, chemical stability, strong corrosion resistance and limited production cost.[11] These substoichiometric titanium oxides are commercially referred to as Ebonex®, with the generic formula of Ti_nO_{2n-1} where n is an integer between 4 and 10.[12] Magnéli phase Ti_4O_7 possesses the highest electrical conductivity (*e.g.*, 1500 S cm^{-1}) as well as comparable or even higher oxidative performance compared with other state-of-the-art electrode materials.[13] These intriguing characteristics indicate that Ti_4O_7 may serve as an alternative electrode material for various environmental applications.

Herein, an electrochemical system composed of a Ti_4O_7 tubular anode and a Pd–Cu co-modified nickel foam (Pd–Cu/NF) cathode was rationally designed. Both are indispensable. The Ti_4O_7 electrode exhibits high stability under high potentials (*e.g.*, 3.0 V *vs.* Ag/AgCl) and may oxidize Cl^- into chlorine

[a]*Textile Pollution Controlling Engineering Center of Ministry of Environmental Protection, College of Environmental Science and Engineering, Donghua University, 2999 North Renmin Road, Shanghai 201620, P. R. China. E-mail: yanbiaoliu@dhu.edu.cn; lifang@dhu.edu.cn*

[b]*Shanghai Institute of Pollution Control and Ecological Security, 1239 Siping Road, Shanghai 200092, P. R. China*

[c]*Instrumental Analysis Center, Donghua University, Shanghai 201620, China*

[d]*State Key Laboratory of Pollution Control and Resource Reuse, School of Environmental Science and Engineering, Tongji University, Shanghai 200092, China*

[e]*Institute of Biosciences, Freiberg University of Mining and Technology, Freiberg 09599, Germany*

† Electronic supplementary information (ESI) available. See DOI: 10.1039/c9ra07470h

radicals (Cl˙). These radicals can rapidly and selectively convert ammonia into N_2 and some by-products (*e.g.*, NO_3^-). In addition, the macro-porous Pd–Cu/NF cathode can effectively reduce NO_3^- and other anodic by-products to N_2.[14] Various advanced characterization techniques were employed to get detailed morphological and compositional information about these electrode materials. The effects of several key parameters on ammonia conversion were also studied. To the best of our knowledge, no reports are available on the rapid and selective electrochemical transformation of ammonia by a Cl˙-mediated Ti_4O_7 electrode. This study provides an efficient and economical method for the treatment of ammonia wastewater.

2. Materials and methods

2.1 Chemicals and materials

Ti_4O_7 electrodes with an inner diameter of 20 mm were purchased from Vector Corrosion Technologies (Ontario, Canada) and were cut into typical lengths of 5 cm before use. Carbon rods with a diameter of 4.0 mm were provided by Shenbei Changfeng Carbon Rod Co., Ltd (Shanghai, China). Nickel foam (NF, 0.5 mm thickness) was purchased from Lizhiyuan Electronics Co., Ltd (China). Sulfuric acid (H_2SO_4, 96–98%), acetone (≥99.5%), palladium(II) chloride ($PdCl_2$, ≥98%), copper(II) sulfate pentahydrate ($CuSO_4 \cdot 5H_2O$, ≥99%), hydrochloric acid (HCl, 36–38%), sodium hydroxide (NaOH, ≥96%), nitric acid (HNO_3, ≥90%), ammonium sulfate ($(NH_4)_2SO_4$, ≥99%) and sodium chloride (NaCl, ≥99.5%) were purchased from Sinopharm Chemical Reagent Co., Ltd. (China). All chemicals were reagent-grade and all solutions were made from DI water with a resistivity of 18.25 MΩ cm.

2.2 Analytical methods

The surface morphology and crystallinity of the Ti_4O_7 electrode was examined by a field emission scanning electron microscope (FESEM, Model No.: Hitachi S-4800, Japan) and an X-ray diffractometer (XRD, Model No.: Rigaku D/max-2550/PC), respectively. X-ray photoelectron spectroscopy was obtained from a Thermo Fisher Scientific Escalab 250Xi X-ray Photoelectron Spectrometer (XPS) under high vacuum (1×10^{-9} torr). The total organic carbon of real water samples was measured with a multi N/C 2100 TOC Analyzer (Analytik Jena AG, Germany). An MS5000 spectrometer (Freiberg Instruments Inc., Germany) was employed to obtain the electron paramagnetic resonance (EPR) spectra using 5,5-dimethyl-1-pyrroline-*N*-oxide (DMPO) as a radical trap. Ammonia concentration was measured by the Nessler reagent method[15] using a TU-1810 UV-vis spectrophotometer (Yixin Instruments Equipment Co., Ltd., Shenzhen) at a wavelength of 420 nm. The amount of N_2 produced was calculated from the total nitrogen (30 mg L^{-1} ammonia) minus the measured concentration of ammonia and nitrate. NO_3^- and NO_2^- concentrations were determined with a DionexTM ICS-5000 ion chromatography system (IC, Thermo Fisher, USA). NB concentration was quantified by a waters 3000 high performance liquid chromatography system (UHPLC, USA) coupled with a C18 column at 262 nm.

2.3 Fabrication of the Pd–Cu/NF cathode

The fabrication of a Pd–Cu/NF electrode followed a previously reported electrodeposition method.[14,16] Briefly, the NF support was cleaned by sequential sonication in H_2SO_4, acetone, and DI water to remove the surface oxidized layer before use. The electrolyte solution consisted of 2 mM $PdCl_2$, 4 mM $CuSO_4 \cdot 5H_2O$ and 0.1 M HCl. The electrodeposition experiment was conducted in a typical three-electrode system using an NF working electrode, a Pt counter electrode, and a saturated Ag/AgCl electrode reference. The deposition potential was controlled at −1.0 V *vs.* Ag/AgCl for 30 min using a CHI 760E electrochemical workstation.

2.4 Electrochemical experiments

The ammonia oxidation experiment was performed in flow-by mode (Fig. S1†) using a Ti_4O_7 tube and a Pd–Cu/NF or a carbon rod cathode. The cathode was arranged at the center of the Ti_4O_7 tube and sealed with silicone rubber to avoid any leakage (Fig. 1). In a typical experiment, 30 mL of 30 mg L^{-1} $(NH_4)_2SO_4$ solution with certain NaCl electrolyte was passed through the reactor and returned. The flow rate (2–6 mL min^{-1}) was controlled by an ISM833C-230V peristaltic pump (Cole-Parmer, USA). Besides the flow circulation, no other mixing was provided in the reactor. The cell potential (1.5–3.2 V *vs.* Ag/AgCl) was provided by a CHI 760E electrochemical workstation. Cyclic voltammetry (CV) experiments were performed using a three-electrode system with a Ti_4O_7 working electrode, a saturated Ag/AgCl electrode reference electrode and a carbon rod counter electrode. The scan rate was set at 20 mV s^{-1} using 0.12 M NaCl or 0.12 M Na_2SO_4 electrolyte.

3. Results and discussion

The surface morphology of the Ti_4O_7 tubular electrode was firstly characterized by FESEM. The results showed that the internal surface of the Ti_4O_7 tubular electrode presented a typical interconnected porous structure (Fig. S2a†). The

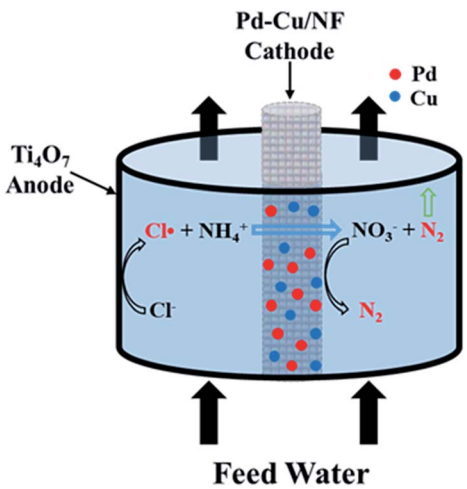

Fig. 1 Schematic of the proposed electrochemical system.

average pore size was determined to be 2.9 ± 0.62 μm (Fig. S2b†). The macropores provide sufficient electroactive sites and are beneficial for the mass transport of target molecules.[17] XRD patterns of the tubular electrode agree well with the Magnéli phase Ti_4O_7 standard pattern[18] (Fig. S3†). This confirmed that the main component of the anode was Ti_4O_7. The XPS technique clearly demonstrated the presence of characteristic peaks of O 1s, Ti 2p and C 1s, with a superficial elemental ratio of 53.4% O, 24.3% Ti and 22.3% C (Fig. S4a†). Two Ti 2p characteristic peaks centred at binding energies of 459 eV ($2p_{3/2}$) and 464.6 eV ($2p_{1/2}$) can be assigned to Ti^{4+} and those observed at 456.2 eV ($2p_{3/2}$) and 461.9 eV ($2p_{1/2}$) can be assigned to Ti^{3+} (Fig. S4b†).[19,20] The cathodic Pd–Cu/NF exhibited a cross-linked grid structure with certain visible particle agglomerations on the NF surface (Fig. S5†). NF showed three characteristic XRD peaks centred at 44.5°, 51.8°, and 76.4°. A typical Pd peak was observed at 40.1° (Fig. S6†).[21] However, no characteristic diffraction of Cu was observed. This may be due to the low crystallinity of the copper phase and the peaks centred at 42° and 48° of the Cu_3Pd phase being masked by the strong peak of Ni at 44.5°.[22] The presence of Pd and Cu elements on NF can also be verified by the XPS technique. The binding energies of the spin–orbit coupling of the metal (Pd^0) were at 340.5 and 335.2 eV, respectively. Another pair of Pd^{2+} signals was observed at 342.2 and 337.0 eV (Fig. S7a†). The Cu 2p spectrum centred at 931.8, 934.4, and 942.7 eV, is attributed to the presence of Cu^0, Cu^+, and Cu^{2+}, respectively[14] (Fig. S7b†).

The anodic potential is an essential factor affecting the ammonia conversion performance. As can be seen from Fig. 2a, only negligible ammonia conversion was observed at an anode potential of 1.5 or 2.0 V *vs.* Ag/AgCl (<3%). Once the anode potential increased to 2.5 V *vs.* Ag/AgCl, a decreased concentration of ammonia was observed, indicating that an ammonia oxidation reaction had occurred. This may be explained by the occurrence of mono-electron chlorine oxidation ($E^0 = 2.4$ V *vs.* NHE) under these conditions (eqn (1)).[23] The as-produced $Cl^{\bullet}$ may selectively react with ammonia to produce NO_3^- or N_2. The ammonia removal performance increased with the anode potential, and complete ammonia transformation within 40 min was observed at an applied anode potential of 3.0 V *vs.* Ag/AgCl. This indicates that the ammonia conversion efficiency could be improved by increasing the applied voltage. Further increasing the anode potential to 3.2 V *vs.* Ag/AgCl did not further accelerate the ammonia oxidation kinetics, which may be due to the occurrence of other side reactions, like water splitting. This may produce gas bubbles, *e.g.* O_2, at the anode surface, blocking the surface-active sites. To alleviate such negative consequences, we adopted an upflow configuration of the reactor. An increased flow rate (*e.g.*, 4 mL min^{-1}) also facilitates the rapid sweeping out of bubbles.[24,25] Therefore, 3.0 V *vs.* Ag/AgCl was selected as optimal for subsequent investigations.

The [Cl^-] was another key parameter impacting the ammonia conversion.[26] As can be seen from Fig. 2b, the ammonia conversion rate increased with increasing [Cl^-] from 0.08 M to 0.12 M. This may be attributed to the production of more chloride radicals with increased [Cl^-]. However, further increasing the [Cl^-] to 0.14 M caused a slight decline in ammonia oxidation efficiency. Excessive [Cl^-] may cause unnecessary side reactions (eqn (2) and (3)) leading to the consumption of $Cl^{\bullet}$ as well as a decreased ammonia conversion efficiency.

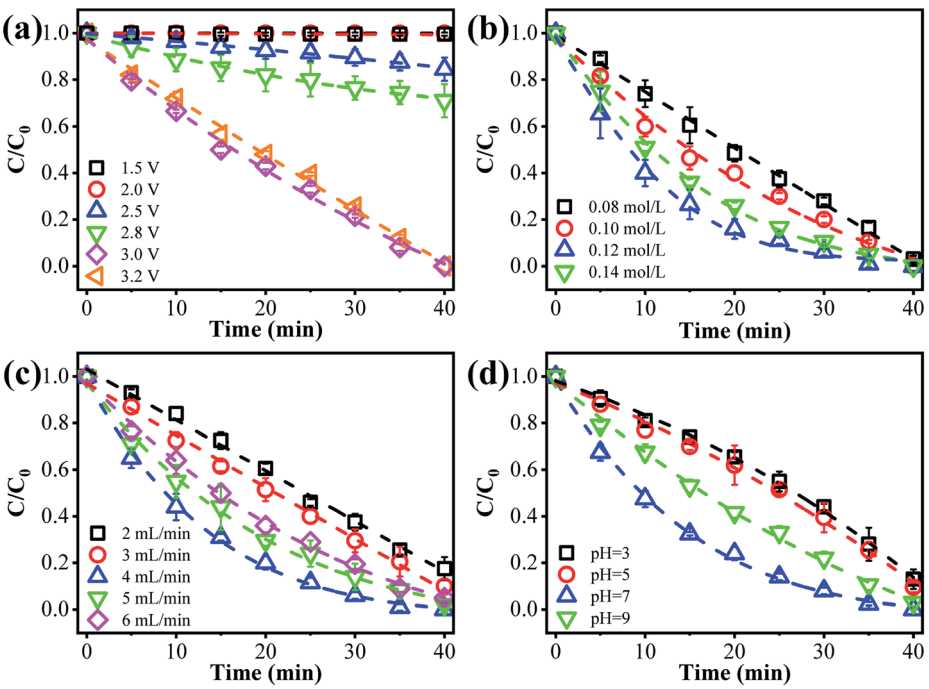

Fig. 2 The effect of different operational factors on ammonia removal: impact of (a) anode potential, (b) [Cl^-], (c) flow rate, and (d) solution pH.

$$Cl^- + h^+(hole) \rightarrow Cl^\bullet \quad (1)$$

$$Cl^\bullet + Cl^- \rightarrow Cl_2^{\bullet-} \quad (2)$$

$$Cl_2^{\bullet-} + H_2O \rightarrow HOCl + Cl^- + H^+ + e^- \quad (3)$$

The flow rate is another important factor.[27,28] As presented in Fig. 2c, the ammonia conversion efficiency increased with flow rate from 2 to 4 mL min^{-1}. This can be explained by the fact that these ammonia ions have more chances to come into contact with these active sites at an increased flow rate in the recirculated filtration mode. Whereas at a flow rate of 6 mL min^{-1}, the ammonia oxidation efficiency showed a decreasing trend. This may be ascribed to the decreased residence time within the reactor (or insufficient contact with the reaction sites) and only an incomplete ammonia oxidation was achieved. We thus chose an optimal flow rate of 4 mL min^{-1} for subsequent study, considering the "trade-off" effect between flow rate and residence time of ammonia.

The impact of solution pH on ammonia conversion was further studied under optimized experimental conditions. Interestingly, as shown in Fig. 2d, the best ammonia conversion performance was obtained at neutral pH. For example, over 40 min of continuous filtration reaction, complete ammonia conversion was obtained at pH 7. Whereas only 87%, 90% and 96% were achieved at pH values of 3, 5, and 9, respectively. This indicates that the designed electrochemical system has great prospects for the treatment of environmental water matrixes. The pH-dependent equilibrium between NH_3 and NH_4^+ is responsible for the increase in ammonia conversion at neutral pH. According to a previous report,[29] ammonia in aqueous solution can exist in either un-ionized form (NH_3) or ionized form (NH_4^+). In these two forms of ammonia, the un-ionized one is more susceptible to oxidation and more abundant under neutral pH conditions. Similar results were previously reported by Zhu *et al.*,[30] who found that NH_3–N was completely removed in a neutral solution but hardly removed in an acidic solution. Conversely, Ji *et al.*[31] reported a highly selective method for transforming ammonia to N_2, based on a novel solar-driven photoelectrochemical coupled chlorine radical reaction system, in which the ammonia removal efficiency was enhanced when the solution acidity increased from pH 6 to 2.

The impact of different operation systems on the conversion of ammonia was further investigated. As presented in Fig. S8,† compared with a conventional batch reactor, the present continuous-flow system demonstrated obviously enhanced kinetics (>99.9% *vs.* 62.3%). This could be due to the convection-enhanced mass transport within the proposed electrochemical system, while diffusion alone dominates the mass transport within the batch system. Moreover, the as-produced gas bubbles may easily block the surface-active sites within the batch reactor, further damaging the overall performance.

The $Cl^\bullet$ can be produced by direct oxidation by Ti_4O_7 or through the instantaneous adduct of Cl^- with $OH^\bullet$.[32] While other side reactions may also consume $Cl^\bullet$, such as $Cl^\bullet$ reacting with Cl^- to form $Cl_2^{\bullet-}$ and further reacting to produce HOCl/OCl^- (eqn (2)–(4)). It is known that $OH^\bullet$, $Cl^\bullet$ and HClO are strong oxidants that can react with NH_4^+.[16] In particular, the $Cl^\bullet$ could react selectively with NH_4^+ ($k_{Cl^\bullet} = 5 \times 10^{13}$ M^{-1} s^{-1})[33] with a much higher reaction rate compared with that of $OH^\bullet$ ($k_{OH^\bullet} = 3 \times 10^8$ M^{-1} s^{-1}).[34] These $Cl^\bullet$ can selectively convert NH_4^+ into N_2, NO_3^- or NO_2^- (eqn (5)–(7)). However, the contribution of ammonia conversion from other reactive chlorine species cannot be eliminated, which will be discussed later.

$$HClO \Leftrightarrow ClO^- + H^+ \quad (4)$$

$$2NH_4^+ + 6Cl^\bullet \rightarrow N_2 + 6Cl^- + 8H^+ \quad (5)$$

$$NH_4^+ + 8Cl^\bullet + 3H_2O \rightarrow NO_3^- + 8Cl^- + 10H^+ \quad (6)$$

$$NH_4^+ + 6Cl^\bullet + 2H_2O \rightarrow NO_2^- + 6Cl^- + 8H^+ \quad (7)$$

The changes in ammonia conversion products over time were investigated under an optimized anode potential of 3.0 V *vs.* Ag/AgCl, [Cl^-] of 0.12 M, flow rate of 4 mL min^{-1} and pH of 7. As shown in Fig. 3a, NO_3^- and N_2 content increased gradually with time to 12 mg L^{-1} and 18 mg L^{-1}, respectively, over 40 min when using a carbon rod cathode. NO_2^- was not detected during this process, possibly due to the strong oxidative ability of Ti_4O_7. However, the ideal product of the present system is N_2, rather than NO_3^-. Since NO_3^- is negatively charged, it has a strong electrostatic repulsion from the cathode surface. Moreover, these NO_3^- ions can also be converted back to NH_4^+ (eqn (8)).[35]

$$NO_3^- + 7H_2O + 8e^- \rightarrow NH_4^+ + 10OH^- \quad (8)$$

To address this issue, a Pd–Cu/NF cathode was further employed to replace the carbon rod cathode.[16] NF, with excellent electrical conductivity and a three-dimensional network, is considered to be a promising cathode material.[14] Moreover, Pd and Cu have been proven to be effective promoters for NO_3^- reduction reaction to N_2.[36] In a recent study, a Pd–Cu/NF cathode demonstrated an evidently enhanced N_2 yield compared with a Pd/NF or a Cu/NF cathode in an SnO_2-CNT based electrochemical system.[14] Importantly, the as-fabricated Pd–Cu/NF surface is positively charged. Hence, the negatively-charged NO_3^- can be easily absorbed onto the cathode surface *via* electrostatic attraction. Therefore, another set of experiments was performed using the Pd–Cu/NF cathode coupled with the Ti_4O_7 anode. The results showed that ammonia was gradually converted to NO_3^- and N_2 over time. Compared with the carbon rod cathode, the NO_3^- removal rate increased by 50% over 40 min of reaction when using the Pd–Cu/NF cathode (Fig. 3b). In addition, Pd and Cu coatings are also essential. The results indicate that similar ammonia removal rates can be obtained with Pd/NF or Cu/NF cathodes. However, the presence of Pd or Cu alone only partially contributed to the conversion of NO_3^- to N_2 (Fig. S9†). This confirmed the capacitive characteristics of the Pd–Cu/NF electrode, which can rapidly adsorb NO_3^- onto the cathode *via* electrostatic attraction. NO_3^- can be reduced to NO_2^- after

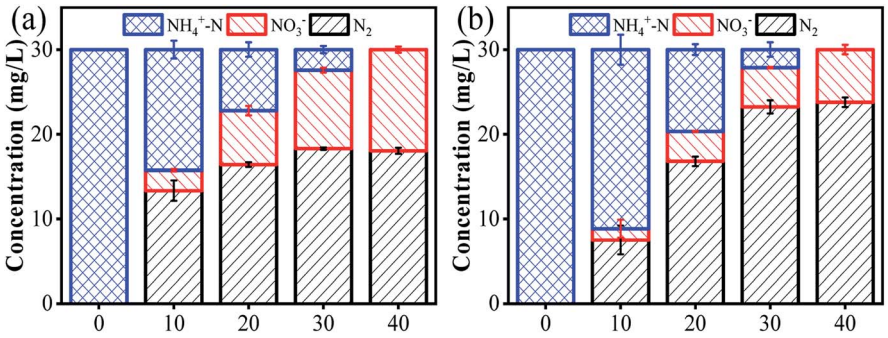

Fig. 3 The conversion of ammonia in 40 min by employing different cathode materials: (a) carbon rod, and (b) Pd–Cu/NF. Reaction conditions: anode potential of 3.0 V *vs.* Ag/AgCl, [Cl^-] of 0.12 M, flow rate of 4 mL min^{-1}, and pH of 7.

adsorption on the Cu site, and then further reduced to N_2 on the Pd site (eqn (9)–(12)).

$$NO_3^- + Cu \leftrightarrow Cu - NO_{3ads}^- \quad (9)$$

$$Cu - NO_{3ads}^- + H_2O + 2e^- \rightarrow NO_2^- + Cu + 2OH^- \quad (10)$$

$$NO_2^- + Pd \leftrightarrow Pd - NO_{2ads}^- \quad (11)$$

$$2Pd - NO_{2ads}^- + 4H_2O + 6e^- \rightarrow N_2 + 2Pd + 8OH^- \quad (12)$$

To distinguish the dominant active species on ammonia conversion, we spiked a few scavengers into the ammonia solution before flowing it into the reactor. We chose nitrobenzene (NB) as an $OH^\bullet$ quenching agent with a k of 3.9×10^9 M^{-1} s^{-1} and *tert*-butanol (*t*BuOH) as a joint quenching agent of $Cl^\bullet$ and $OH^\bullet$ with k values of 1.9×10^9 and 6×10^8 M^{-1} s^{-1}, respectively.[37] As shown in Fig. 4a, complete ammonia conversion was observed within 40 min of reaction in the absence of any scavengers. However, the ammonia conversion decreased by 74% in the presence of *t*BuOH within the same period. This suggests that the ammonia removal process indeed involved radicals and that HOCl plays only a minor role. To quantitatively determine the amount of [$OH^\bullet$], we used an indirect method by adding 1 mM NB into the reaction medium due to their high affinity. According to eqn (13), [$OH^\bullet$] is determined to be 1.06×10^{-11} M with a K_{NB} of 0.04133 min^{-1} (Fig. S10†). While the ammonia conversion decreased by only 17% when NB was added, proving that $Cl^\bullet$ may play a dominant role in the process of ammonia oxidation. It is of note that other radicals such as $NO_3^\bullet$ may also exist in the solution and contribute to ammonia conversion. However, the reaction rate constant of $NO_3^\bullet$ with *t*BuOH ($k = 5.7 \times 10^4$ M^{-1} s^{-1})[38] was 5 orders of magnitude lower than that of $Cl^\bullet$. It is thus reasonable to believe that the contribution from $NO_3^\bullet$ is negligible.

$$K_{NB} = k_{OH^\bullet,NB}[OH^\bullet] \quad (13)$$

The production of $Cl^\bullet$ and $OH^\bullet$ during electrochemical filtration was further determined by the EPR technique. As presented in Fig. 4b, the typical 4-peak spectrum of $OH^\bullet$ with an intensity ratio of 1 : 2 : 2 : 1 was detected with DMPO as a spin trapping agent.[39] However, an alternative 11-peak spectrum was detected at an increased anode potential of 2.5 or 3.0 V *vs.* Ag/AgCl. This 11-peak spectrum can be divided into a 4-peak (DMPO-$OH^\bullet$) signal and another 7-peak signal. According to previous studies, these 7-peak signals may be ascribed to DMPO-Cl, which are enhanced with an applied potential up to 3.0 V *vs.* Ag/AgCl[40] (Fig. S11†). Similar results were previously

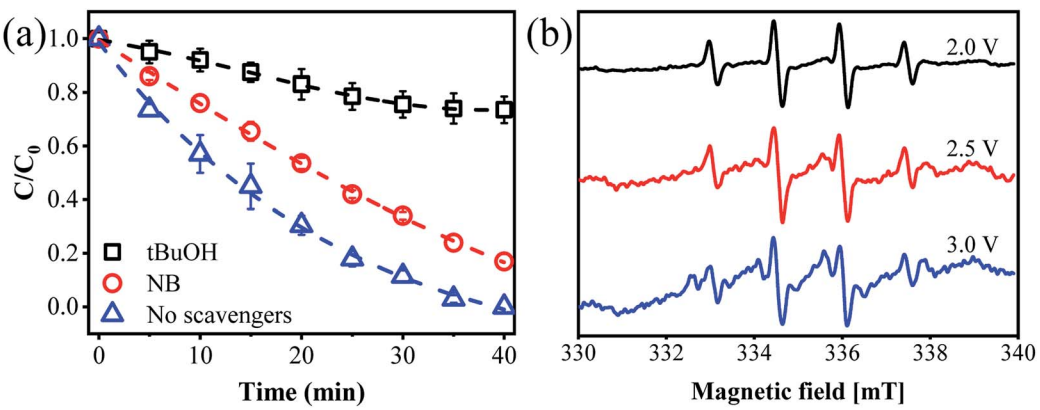

Fig. 4 (a) Effect of different scavengers on ammonia removal. (b) EPR spectra with DMPO observed from the flow-by experiment at different applied anode potentials.

reported by Li *et al.*[14] This confirmed the formation of OH$^{\bullet}$ and Cl$^{\bullet}$ within the present electrochemical flow-by system. In addition, we performed another control experiment using Na_2SO_4 to replace NaCl. As expected, only negligible ammonia conversion (<5%) was observed, regardless of the anode potentials (Fig. S12†), further indicating the essential role of Cl^-. The CV spectrum in 0.12 M of NaCl and Na_2SO_4 solution also indicates that an oxidation reaction occurred at an anode potential of 2.92 V *vs.* Ag/AgCl using an NaCl electrolyte, as evidenced by the obvious oxidative peak. This oxidative peak could be due to the ammonia oxidation reaction in the presence of Cl$^{\bullet}$, while no visible redox peak was observed when using the Na_2SO_4 electrolyte (Fig. S13†). This indirectly verifies the essential role of Cl$^{\bullet}$ for ammonia transformation in this reaction system.

To examine the potential applications of the proposed system, ammonia conversion with different background solutions was investigated. To do this, 30 mg L^{-1} of $(NH_4)_2SO_4$ were added to local tap and lake water samples before flowing into the electrochemical system. A similar conversion trend for ammonia was observed in all cases (Fig. S14†). Complete ammonia conversion could still be obtained in tap water with a background total organic carbon (TOC) of 1.8 mg L^{-1}. In addition, the removal of ammonia was about 97% when challenged with lake water with a background TOC of 93.2 mg L^{-1}. The effect of selected common anions (*e.g.*, carbonate, phosphate and silicate) on ammonia conversion was further investigated under optimal operating conditions (Fig. S15†). The results showed that such inhibition was negligible in the presence of carbonate at varying concentrations. Silicate and phosphate posed a slight inhibitory effect on ammonia conversion. When the concentration increased from 5 to 20 mM, the ammonia conversion efficiency decreased from 100% to 86.5% and 82.3%, respectively. This indicates that the complex composition of natural water and the presence of some competitive ions produces only negligible inhibition of ammonia conversion. This result can be explained by the fact that the Cl$^{\bullet}$ react selectively with other electron-rich groups (*e.g.*, NH_4^+). The stability of Ti_4O_7 was further evaluated by performing four consecutive cycles of ammonia removal experiments in DI-H_2O conditions. The results showed an average 98.7 $\pm$ 2.2% ammonia removal efficiency, indicating the excellent anodic stability of the Ti_4O_7 electrode (Fig. S16†). These positive outcomes indicate that the proposed electrochemical system is a potential technology for removing ammonia from various water environments. It should be noted that the toxicity of Cl$^{\bullet}$ is beyond the scope of this work. We would like to leave this key question for further exploration.

4. Conclusions

In summary, a continuous-flow electrochemical system was developed towards effective and exhaustive ammonia removal. The proposed electrochemical system employs a highly stable tubular Magnéli phase Ti_4O_7 anode coupled with a Pd–Cu co-modified NF cathode. The as-produced Cl$^{\bullet}$ can react selectively with NH_4^+ to produce N_2 as it flows through the electrochemical system. This flow-by electrochemical system also demonstrated enhanced oxidative kinetics compared with a conventional batch system.

Conflicts of interest

There are no conflicts to declare.

Acknowledgements

This work was supported by the Natural Science Foundation of Shanghai, China (No. 18ZR1401000), the Fundamental Research Funds for the Central Universities (No. 2232019G-11), and the Shanghai Pujiang Program (No. 18PJ1400400).

References

1 S. Y. Weon, S. I. Lee and B. Koopman, *Environ. Technol.*, 2004, **25**, 1211–1219.
2 L. Chmielarz and M. Jablonska, *RSC Adv.*, 2015, **5**, 43408–43431.
3 Z. J. Li, X. P. Zhang, H. F. Dong, X. C. Zhang, H. S. Gao, S. J. Zhang, J. W. Li and C. M. Wang, *RSC Adv.*, 2015, **5**, 81362–81370.
4 W. J. Tang, Y. Zhang, J. Bai, J. H. Li, J. C. Wang, L. S. Li, T. S. Zhou, S. Chen, M. Rahim and B. X. Zhou, *Sep. Purif. Technol.*, 2020, **234**, 9.
5 J. Lee, H. Park and W. Choi, *Environ. Sci. Technol.*, 2002, **36**, 5462–5468.
6 X. R. Zhang, W. G. Li, E. R. Blatchley, X. J. Wang and P. F. Ren, *Water Res.*, 2015, **68**, 804–811.
7 Y. Y. Xiang, J. Y. Fang and C. Shang, *Water Res.*, 2016, **90**, 301–308.
8 Y. Yang, J. J. Pignatello, J. Ma and W. A. Mitch, *Environ. Sci. Technol.*, 2014, **48**, 2344–2351.
9 F. Li, X. Peng, Y. B. Liu, J. C. Mei, L. W. Sun, C. S. Shen, C. Y. Ma, M. H. Huang, Z. W. Wang and W. G. Sand, *Chemosphere*, 2019, **229**, 383–391.
10 C. Y. Zhang, D. He, J. X. Ma and T. D. Waite, *Water Res.*, 2018, **145**, 220–230.
11 F. C. Walsh and R. G. A. Wills, *Electrochim. Acta*, 2010, **55**, 6342–6351.
12 S. Nayak and B. P. Chaplin, *Electrochim. Acta*, 2018, **263**, 299–310.
13 C. Trellu, C. Coetsier, J. C. Rouch, R. Esmilaire, M. Cretin and C. Causserand, *Water Res.*, 2017, **131**, 310–319.
14 F. Li, X. Peng, Y. B. Liu, J. Mei, L. Sun, C. Shen, C. Ma, M. Huang, Z. Wang and W. Sand, *Chemosphere*, 2019, **229**, 383–391.
15 K. Fang, H. Gong, W. Y. He, F. Peng, C. H. He and K. J. Wang, *Chem. Eng. J.*, 2018, **348**, 301–309.
16 Y. Zhang, J. Li, J. Bai, Z. Shen, L. Li, L. Xia, S. Chen and B. Zhou, *Environ. Sci. Technol.*, 2018, **52**, 1413–1420.
17 L. J. J. Janssen and L. Koene, *Chem. Eng. J.*, 2002, **85**, 137–146.
18 L. Guo, Y. Jing and B. P. Chaplin, *Environ. Sci. Technol.*, 2016, **50**, 1428–1436.

19 X. Y. Tao, J. G. Wang, Z. G. Ying, Q. Cai, G. Zheng, Y. Gan, H. Huang, Y. Xia, C. Liang, W. Zhang and Y. Cui, *Nano Lett.*, 2014, **14**, 5288–5294.
20 X. X. Li, A. L. Zhu, W. Qu, H. Wang, R. Hui, L. Zhang and J. Zhang, *Electrochim. Acta*, 2010, **55**, 5891–5898.
21 Z. Q. Zhang, Y. P. Xu, W. X. Shi, W. Wang, R. J. Zhang, X. Bao, B. Zhang, L. Li and F. Y. Cui, *Chem. Eng. J.*, 2016, **290**, 201–208.
22 Y. Yoshinaga, T. Akita, I. Mikami and T. Okuhara, *J. Catal.*, 2002, **207**, 37–45.
23 C. D. Vecitis, M. H. Schnoor, M. S. Rahaman, J. D. Schiffman and M. Elimelech, *Environ. Sci. Technol.*, 2011, **45**, 3672–3679.
24 P. Gayen, C. Chen, J. T. Abiade and B. P. Chaplin, *Environ. Sci. Technol.*, 2018, **52**, 12675–12684.
25 T. X. H. Le, H. Haflich, A. D. Shah and B. P. Chaplin, *Environ. Sci. Technol. Lett.*, 2019, **6**, 504–510.
26 J. Ding, Q. L. Zhao, J. Q. Jiang, L. Wei, K. Wang, Y. Zhang, W. Hou and H. Yu, *Environ. Sci. Pollut. Res.*, 2017, **24**, 5152–5158.
27 K. W. Kim, Y. J. Kim, I. T. Kim, G. I. Park and E. H. Lee, *Electrochim. Acta*, 2005, **50**, 4356–4364.
28 Y. B. Liu, P. Wu, F. Q. Liu, F. Li, X. An, J. Liu, Z. Wang, C. Shen and W. Sand, *Environ. Sci. Technol.*, 2019, **53**, 1527–1535.
29 S. H. Lin and C. L. Wu, *Water Res.*, 1996, **30**, 715–721.
30 X. Zhu, J. Ni and P. Lai, *Water Res.*, 2009, **43**, 4347–4355.
31 Y. Z. Ji, J. Bai, J. H. Li, T. Luo, L. Qiao, Q. Zeng and B. Zhou, *Water Res.*, 2017, **125**, 512–519.
32 B. P. Chaplin, *Acc. Chem. Res.*, 2019, **52**, 596–604.
33 Y. D. Gao, I. M. Alecu, P. C. Hsieh, B. P. Morgan, P. Marshall and L. N. Krasnoperov, *J. Phys. Chem. A*, 2006, **110**, 6844–6850.
34 L. Jing, B. Chen, D. Y. Wen, J. S. Zheng and B. Y. Zhang, *Environ. Sci. Pollut. Res.*, 2018, **25**, 2691–2701.
35 X. R. Zhang, W. G. Li, E. R. Blatchley III, X. Wang and P. Ren, *Water Res.*, 2015, **68**, 804–811.
36 Y. Wang, J. H. Qu and H. J. Liu, *Chin. Chem. Lett.*, 2006, **17**, 61–64.
37 M. J. Watts and K. G. Linden, *Water Res.*, 2007, **41**, 2871–2878.
38 S. P. Mezyk, T. D. Cullen, K. A. Rickman and B. J. Mincher, *Int. J. Chem. Kinet.*, 2017, **49**, 635–642.
39 X. R. Wang, Y. Li, L. P. Tang, W. Gan, W. Zhou, Y. F. Zhao and D. S. Bai, *Chin. Chem. Lett.*, 2017, **28**, 394–399.
40 T. Li, Y. Jiang, X. Q. An, H. Liu, C. Hu and J. Qu, *Water Res.*, 2016, **102**, 421–427.